IEEE Access
Multidisciplinary ⋮ Rapid Review ⋮ Open Access Journal

Received November 16, 2021, accepted November 27, 2021, date of publication November 30, 2021,
date of current version December 15, 2021.

Digital Object Identifier 10.1109/ACCESS.2021.3131681

A Comparative Study on Model Predictive Control Design for Highway Car-Following Scenarios: Space-Domain and Time-Domain Model

YOUNGRO LEE[1], (Student Member, IEEE), DAE YOUNG LEE[1], (Member, IEEE), SEUNG HWAN LEE[2], (Member, IEEE), AND YOUNGKI KIM[3], (Member, IEEE)

[1]Department of Aerospace Engineering, Iowa State University, Ames, IA 50011, USA
[2]Department of Mechanical Engineering, Hanyang University, Seoul 04763, South Korea
[3]Department of Mechanical Engineering, University of Michigan–Dearborn, Dearborn, MI 48128, USA

Corresponding authors: Dae Young Lee (daylee@iastate.edu) and Seung Hwan Lee (seunghlee@hanyang.ac.kr)

This work was supported in part by the Korea Institute of Energy Technology Evaluation and Planning (KETEP), and in part by the Ministry of Trade, Industry and Energy (MOTIE) of South Korea under Grant 20213030030190.

ABSTRACT Model predictive control (MPC) has been widely adopted for cooperative adaptive cruise control (CACC) due to its superior performance in achieving fuel-efficient driving while satisfying constraints such as inter-vehicle distance. The core of an MPC-based algorithm is to predict the vehicle's behavior using a dynamic model, and the space-domain vehicle dynamic model is frequently implemented in recent research along with the time-domain vehicle dynamic model. This paper presents a comparative performance analysis between the space-domain and the time-domain models in the MPC framework for the car-following problem. An MPC design process and analysis method for the high-speed car-following scenario is suggested and presented for equivalent performance comparison between the two approaches. In order to analyze trends between speed tracking and fuel-saving performance, which are conflicting objectives as car-following performance, a bi-objective cost function is proposed and manipulated by various weightings. It is observed that the space-domain model presents stable tracking performance, and the time-domain model shows better fuel efficiency. However, the space-domain model with road information is superior in tracking and fuel efficiency compared to the time-domain model with limited road information. Pareto analysis was implemented to visualize and describe performance differences in various situations regarding tracking error, fuel efficiency, and road grade information levels.

INDEX TERMS Cooperative adaptive cruise control, car-following problem, model predictive control, multi-objective optimization.

I. INTRODUCTION

The car-following problem with an autonomous driving system has been actively researched because of increased attention and advancement in cooperative adaptive cruise control (CACC) with a real-time control system. Among the various approaches to the car-following problem, Model Predictive Control (MPC) has been widely adopted for its constraint handling capability and optimal solutions [1]–[4]. Even though MPC-based CACC requires high computational power and vehicle-to-vehicle communication (V2V), the latest advances in embedded processors and communication technologies enable simple implementation [1], [5]–[7].

The associate editor coordinating the review of this manuscript and approving it for publication was Ton Duc Do.

The essence of MPC is to handle multi-objective cost functions and state/input constraints by predicting the future behavior of a system. For instance, MPC-based approaches in [8], [9] perform fuel-efficient driving while considering the signal and traffic status of the upcoming intersections. In [10], [11], researchers merged heading road information, such as road grade and curvature to achieve advanced fuel efficiency. Likewise, in the car-following problem, the MPC technique can improve fuel consumption, tracking error, riding comfort, and accomplish defensive and ecological driving by predicting the behavior of vehicles and satisfying various constraints [12]–[16].

As examined in these MPC applications, the vehicle dynamics model is necessary to predict the vehicle's behavior, and a majority of CACC applications have been utilizing the conventional modeling evolving in the time domain [2],

[8], [17]–[21]. However, since the road information, such as grade and curvature, is usually a function of position, the time-domain vehicle model needs additional position estimation to exploit the road grade for the prediction, which usually causes estimation errors [2]. This position error degrades the accuracy of road information and increases uncertainties in driving and constraints handling, making energy-efficient driving challenging [22]. Because of this challenge, some CACC works based on the time-domain vehicle model [3], [23] assume flat road or constant grade conditions when predicting the vehicles' behavior; thus, the difference between time-domain and space-domain vehicle models emerges.

Many researchers recently have started to actively use the space-domain vehicle model in order to take advantage of road grade information [9], [10], [24]–[28], which can be acquired easily than before via the global positioning system (GPS) [29], [30]. Since the road grade significantly influences the control sequences, knowing the future road information has a significant advantage in reducing disturbances and errors in vehicle behavior prediction [2]. More accurate estimation of the rolling and grading resistance from the road information enables the MPC-based algorithm to compute the optimal control sequence [30]. Besides the more accurate road information, another benefit of the space-domain model is that the position of the ego vehicle can be omitted in the state vector of the vehicle dynamics, thus mitigating the computational burden of the controller [31]. However, since the space-domain model updates the vehicle's state by calculating a square root term, the optimizer needs to handle the additional computation burden or inaccuracy in the solution [32]. On the other hand, the time-domain model can be a linear equation that guarantees reduced computation burden but decreases prediction accuracy by ignoring resistance forces. In [2], it is mentioned that safety constraints in the car-following problem can be handled more easily in the time domain, but this paper suggests that their argument depends on the case.

As described, the time-domain and space-domain vehicle models have their pros and cons. However, to the best of the authors' knowledge, there has been no comparative study examining the performance difference between domain vehicle models. To fill this gap, this paper constructs two MPC frameworks based on the time-domain and space-domain vehicle models and suggests a comparison method to reveal the difference between the two MPC frameworks.

Many pieces of MPC-based work focus on reducing fuel consumption during the car-following or vehicle platooning scenarios [5], [10], [33], [34]. For fuel-efficient driving, some works construct a cost-function only with a stand-alone fuel consumption model [25], [35], [36], and others exploit a multi-objective cost function [2], [37]–[39], [39], [40]. Note that the strategy of minimizing fuel consumption usually results in the ego vehicle drifting away from the preceding vehicle within the boundary of inter-vehicle distance, so it contradicts with reducing tracking errors. To explore a trade-off between speed tracking performance and fuel consumption when inter-vehicle distance constraints exist, we adopt a bi-objective cost function comprised of speed tracking error and desired acceleration. Distinctive features of each MPC framework are identified by a relative weighting between the two objectives. Furthermore, macroscopic trends of the optimal solutions are examined using the concept of Pareto optimality [41] that presents a trade-off in the bi-objective optimization problem with different road grade information.

In this paper, a highway car-following scenario with inter-vehicle distance constraints is considered for the numerical simulations. The reason we focused on the highway scenario is that it makes the simulation focus on presenting fuel efficiency and tracking performance without considering signal and traffic status. In car-following scenarios, the inter-vehicle distance is typically regulated by the time headway boundary [30], [42]. However, depending on which domain model is adopted, the headway boundary should be implemented differently. Because the time-domain model uses time as an independent variable, it cannot explicitly be expressed in the state vector but only inferred by the steps. In the case of the space-domain model, the relation is just the opposite and the headway is explicitly expressed in the state vector as time, making it easy to track. This paper explains the difference between each model in the headway constraint handling and compares its consequences.

The main contributions of this paper are threefold. First, to enable an equivalent performance comparison between the two approaches, we suggest the methodology, design process, and high-speed car-following scenario. Second, performance differences between the time-domain and space-domain MPC frameworks are analyzed through parametric studies. Specifically, the trade-off trends between fuel efficiency and speed tracking performance that are subject to road grade availability are discussed using Pareto analysis. Third, based on the simulation results and analysis, we suggest which modeling approach is better for different car-following scenarios from a speed tracking and fuel efficiency perspective. To reveal the conclusion, if the inter-vehicle distance is constrained in terms of time headway in the car-following problem, then the space-domain approach can produce a lower speed tracking error compared to the time-domain approach.

The rest of this paper is organized as follows. In section 2, the time-domain and space-domain vehicle models are defined, and a fuel-consumption model is introduced. Section 3 describes the design process of the MPC frameworks for a highway car-following scenario with inter-vehicle distance constraints. Section 4 shows the simulation results of each MPC framework, followed by performance comparison and analysis through obtaining Pareto fronts. Section 5 summarizes and discusses the main results and observations of the paper. Lastly, the conclusion of this paper is made in section 6.

II. MODELING

This section introduces two sets of vehicle longitudinal dynamics models expressed in either time or space domains.

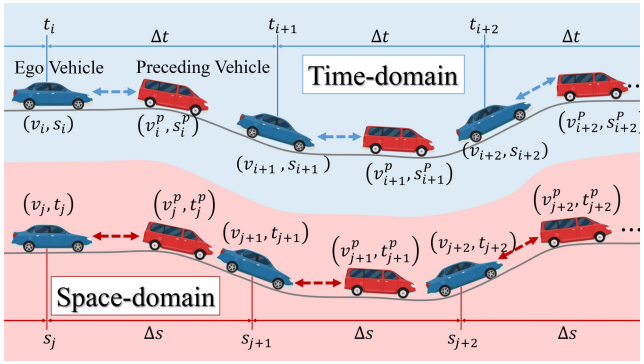

FIGURE 1. Schematic diagram of a car-following scenario using time-domain and space-domain vehicle models.

Although they depict the same phenomena fundamentally, their mathematical expressions differ because they employ different independent variables, either time or space. Hence, a vehicle's state evolves over the corresponding independent variable according to the employed domain. The continuous vehicle dynamics is discretized using a zero-order-hold conversion, and propagated numerically using the forward Euler method [18], [21], [43]–[45]. To mitigate the numerical error from the discretization and integration methods, we adopt a 0.2 second sampling interval which is smaller than the values in the references. In addition to the dynamic models, a fuel consumption model, which provides a reasonable estimation of fuel consumption based on the speed and acceleration of the ego vehicle at each step, is introduced. The total fuel consumption of each MPC framework can be calculated by accumulating the instantaneous fuel consumption, and the performance of each approach will be compared in terms of fuel efficiency.

A. TIME-DOMAIN VEHICLE MODEL

As can be seen from the upper section of Fig. 1, the vehicle's state in the time domain is updated at every time instant. Because the preceding vehicle has a preplanned speed profile for the scenario, only the ego vehicle's motion will be calculated through the time-domain vehicle model, which is defined as

$$a_i = a_{des,i} - \frac{1}{m} R_i, \tag{1a}$$

$$v_{i+1} = v_i + a_i \Delta t, \tag{1b}$$

$$s_{i+1} = s_i + \frac{v_i + v_{i+1}}{2} \Delta t, \tag{1c}$$

where a_i, v_i, and s_i are the acceleration, speed, and distance traveled at each instant, i, respectively, and the sampling time is fixed as Δt. Note that $a_{des,i}$ is the desired acceleration of the ego vehicle, which will be computed through the MPC framework. Note that the distance traveled at every instant, s_i, is calculated to evaluate the safe distance between the ego and preceding vehicles. If there is no safety constraint to consider, then the computation of the distance traveled is unnecessary.

Resistance forces acting on the ego vehicle, R_i, are given by

$$R_i = \frac{1}{2} \rho A C_d {v_i}^2 + C_r mg \cos\theta(s_i) + mg \sin\theta(s_i), \tag{2}$$

where m is the mass of the ego vehicle, g is gravitational acceleration at sea level, A the is front area of the ego vehicle, C_r is the rolling friction coefficient between the ground and wheels, C_d is the aerodynamic drag coefficient, and ρ is the air density at sea level. These six values are considered constants.

Overall, if the time-domain state vector is defined as $x_i \equiv (v_i, s_i)$, the vehicle model in the time domain can be briefly expressed as

$$x_{i+1} = f\left(x_i, a_i, \theta(s_i)\right). \tag{3}$$

Since the road grade, $\theta(s)$, is the position-dependent function, it requires predicting the vehicle position for estimating the corresponding road information at each time instant, and this causes estimation errors [2]. This is one of the major drawbacks of employing the time-domain vehicle model for car-following applications. In the simulation section, how the road information would affect car-following performance will be evaluated by simulations with various information levels of road grade.

B. SPACE-DOMAIN VEHICLE MODEL

The vehicle model expressed in the space domain is given as

$$a_j = a_{des,j} - \frac{1}{m} R_j, \tag{4a}$$

$$v_{j+1} = \sqrt{v_j^2 + 2 a_j \Delta s}, \tag{4b}$$

$$t_{j+1} = t_j + \frac{2\Delta s}{v_{j+1} + v_j}, \tag{4c}$$

where a_j, v_j, and t_j are the acceleration, speed, and elapsed time at each distance instant j, respectively, and the resistance force, R_j, is computed by using (2). Δs is the sampling distance, whose numerical value will be selected to have a similar sampling rate to the time-domain driving cycle. Note that the variables in the space-domain model have the same physical meaning as those in the time-domain model. For example, v_j and a_j are physical quantities that are derivatives with respect to time, not space. Moreover, the elapsed time, t_j, is calculated and saved to constrain the inter-vehicle distance between the ego and preceding vehicles when a certain value of time headway is provided. The space-domain discrete vehicle dynamic model can be briefly expressed as

$$y_{j+1} = f\left(y_j, a_j, \theta(s_j)\right), \tag{5}$$

where the space-domain state vector is defined as $y_j \equiv \left(v_j, t_j\right)$. This expression will be used to construct the space-domain MPC framework.

The space-domain model differ from the time-domain model in two aspects. First, unlike the time-domain model, it consists of nonlinear equations. The square root term in (4b) may induce computational error or require using an additional constraint in the MPC framework to maintain positive

values. In addition, because the speed should be placed on the denominator to calculate the elapsed time, one cannot transform the space-domain vehicle model into a state-space representation. The road grade, illustrated in the bottom of Fig. 1, is position-dependent and therefore easily accessible with the position data.

C. FUEL CONSUMPTION MODEL

To calculate the total amount of fuel consumption of the ego vehicle during the car-following scenario, we adopt the Virginia Tech comprehensive power-based fuel consumption model (VT-CPFM), whose mathematical expression is presented in [46], [47]. Since both (3) and (5) provide the speed and acceleration of the ego vehicle at every time or space instant, we can easily compute instantaneous fuel consumption at the corresponding instance by using the VT-CPFM. The instantaneous fuel consumption, $F_{c,i}$, is modeled as a function of vehicle power, P_i, at every instant.

$$FC_i = \begin{cases} f_0 + f_1 P + f_2 P_i^2, & \forall P_i \geq 0, \\ f_0, & \forall P < 0, \end{cases} \tag{6a}$$

$$P_i = \left(\frac{R_i + 1.04\, ma_i}{3600 \eta_d} \right) v_i, \tag{6b}$$

where f_0, f_1, and f_2 are vehicle model constants that need to be calibrated for each vehicle. The resistance forces, R_i, in the vehicle power calculation are identical to those in (2). Note that instant indices i and j here are interchangeable depending on the adopted domain.

III. MODEL PREDICTIVE CONTROL FRAMEWORKS

In this section, we present two MPC frameworks based on the domain of interest for vehicle modeling: time-domain and space-domain. Then, the control problem in each framework is formulated to minimize speed tracking errors and fuel consumption simultaneously while constraining the inter-vehicle distance. The main distinction between the frameworks is the physical expression of the inter-vehicle distance, which brings differences in the handling of time headway boundary.

A. TIME-DOMAIN MPC FRAMEWORK

The MPC-based car-following problem in the time-domain is designed as

$$\min J_i = \sum_{i=k}^{k+N_p} \left[(1-\omega) \left(v_i - v_i^p \right)^2 + \omega a_{des,i}^2 \right] + c\alpha^2, \tag{7a}$$

$$\text{subject to } x_{i+1} = f\left(x_i, a_i, \theta(s_i)\right), \tag{7b}$$

$$v_{min} \leq v_i \leq v_{max}, \tag{7c}$$

$$a_{min} \leq a_{des,i} \leq a_{max}, \tag{7d}$$

$$v_i t_l^h < s_i^p - s_i < v_i \left(t_u^h + \alpha \right), \tag{7e}$$

where superscript p and N_p refer to the preceding vehicle and predefined prediction horizon, respectively. A strategy commonly solicited in the car-following problem is fuel economy driving, which demands a cost function to carry a fuel consumption model as well as an elaborate engine model. In order to mitigate the computational burden in test runs, the desired acceleration of the ego vehicle is exploited instead. The simulation results in the following section verify that there is a near-linear relationship between acceleration and fuel consumption. In addition, to explore the difference between the time-domain and space-domain models in the MPC framework, we impose a relative weighting between the speed tracking error and the desired acceleration. Different trends of each approach are investigated through a series of simulations where a weighting parameter, ω, varies from 0 to 1.

The inter-vehicle distance between the ego and preceding vehicles is constrained by an induced time headway boundary as indicated in (7e). Since time is an independent variable here, it converts a given time headway boundary into distance information. This conversion causes redundant margins in the inter-vehicle distance, which will be presented in the simulation section. The lower bound, t_l^h, stipulates the minimum safe distance, and the upper bound, t_u^h, is added to prevent the inter-vehicle distance from growing excessively. However, imposing hard constraints on both sides of the boundary of inter-vehicle distance may result in infeasible solutions; thus, we introduce a slack variable α, which is another optimization variable to be implemented through the MPC framework. The slack variable alleviates the upper bound of inter-vehicle distance, turning into a soft constraint. Since the slack variable stays close to zero most of the time, it needs to be multiplied by a large constant, c, so that it can penalize the cost function. The dashed blue arrows in the top of Fig. 1 indicate the inter-vehicle distance (space headway) in the time domain. (7c) and (7d) provide the boundaries of hard constraints on vehicle speed and acceleration.

B. SPACE-DOMAIN MPC FRAMEWORK

The MPC-based car-following problem in the space-domain is constructed as

$$\min J_j = \sum_{j=q}^{q+N_p} \left[(1-\omega) \left(v_j - v_j^p \right)^2 + \omega a_{des,j}^2 \right] + c\alpha^2, \tag{8a}$$

$$\text{subject to } y_{j+1} = f\left(y_j, a_j, \theta(s_j)\right), \tag{8b}$$

$$v_{min} \leq v_j \leq v_{max}, \tag{8c}$$

$$a_{min} \leq a_{des,j} \leq a_{max}, \tag{8d}$$

$$t_l^h < t_j - t_j^p < t_u^h + \alpha. \tag{8e}$$

It has similar a structure as the time-domain MPC framework except for two aspects. First, the most notable difference is the mathematical description of the time headway boundary for constraining the inter-vehicle distance. Since the space-domain vehicle model calculates the elapsed time at every distance instant by using (4c), the boundary condition of the time headway can be directly converted into distance information as indicated in (8e). Hence, it is important to know that the dashed red arrows in Fig. 1 represent the

TABLE 1. Vehicle model and simulation parameter values.

Parameter	Value	Parameter	Value
m	3152 kg	g	9.81 m/s^2
A	3.28 m^2	η_d	0.92
C_d	0.6	f_0	0.0078 L/s
C_r	0.033	f_1	1×10^{-6} L/s $\cdot$ kW
ρ	1.23 kg/m^3	f_2	1.95×10^{-5} L/s $\cdot$ kW^2
Δt	0.2 s	Δs	4.5 m
v_{min}	0 m/s	v_{max}	30 m/s
a_{min}	-2 m/s^2	a_{max}	2 m/s^2
t_l^h	2 s	t_u^h	5 s
N_p	50	N_c	50
c	1000		

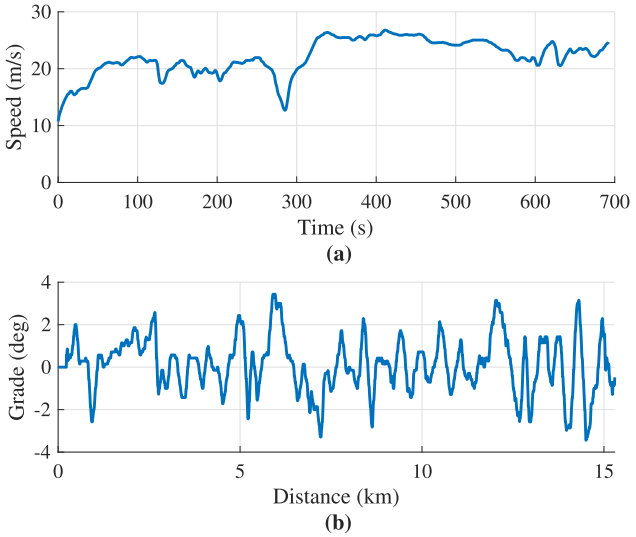

FIGURE 2. Driving cycle and road grade information used for simulations in this paper. (a) HWFET cycle assumed as speed profile of the preceding vehicle. (b) Road grade of US12 utilized as the corresponding road profile for the HWFET cycle.

time headway at each distance instant, not the inter-vehicle distance.

IV. NUMERICAL SIMULATION

Numerical simulations have been performed to evaluate the performance difference between the time-domain and space-domain MPC frameworks in the car-following problem. In this section, the car-following performances of each approach are assessed based on the root-mean-square (RMS) value of speed tracking error, RMS value of desired acceleration, and the time headway.

The simulation parameters are provided in Table 1. The parameters to be utilized in the vehicle model and the fuel consumption model are adopted from [36]. Sampling time and sampling distance are determined as 0.2 second and 4.5 meters, respectively. Those sampling intervals allow the discrete vehicle dynamics to describe the vehicle behavior well. The prediction horizon, N_p, is selected as 50 steps so that the ego vehicle predicts 10 seconds or 225 meters ahead. The control horizon, N_c, is set identically to the prediction horizon. Furthermore, the control frequency is defined identically to the sampling frequency of the driving cycle, so that the receding horizon is shifted for one step every cycle, and the prediction and optimization are repeated until the horizon reaches the end of the driving cycle. The weighting factor, c, is selected as 1000 by trial and error so that the slack variable, α, can penalize the cost function at a level similar to the primary cost values. The lower bound of the time headway follows the two-second rule distributed by the U.S. Department of Transportation [48]–[50], and the upper bound is decided to be five seconds.

In order to improve convergence and computational efficiency, we exploit the warm-start method. Warm-start procedures are designed to discover advanced starting points for optimization in order to reduce the number of iterations needed to get the best result [51]–[53]. The solver calculates an optimal acceleration profile over the prediction horizon, N_p, and implements one control step such that $N_p - 1$ unused solutions still remain. The remaining solutions are utilized as initial guess for the next step's optimization problem.

A nonlinear solver in MATLAB®, fmincon, is adopted to formulate and solve the multi-objective car-following problem. The interior-point method is exploited due to more satisfactory convergence performance and faster computational speed than the SQP method. The simulations are performed using a Windows 10 operating system with a 3.5 GHz 4-core Intel® Xeon® processor and 16 GB DDR4 RAM memory.

A. DRIVING CYCLE

The highway fuel economy test (HWFET) cycle developed by the U.S. environmental protection agency (EPA) is adopted for the preplanned speed profile of the preceding vehicle. Fig. 2 (a) shows the part of the HWFET cycle in which the speed is greater than 10 m/s. We assume a high-speed driving cycle to provide the similar number of samples to both approaches, since sampling time and distance are constant over the driving cycle. In order to find out the influence of the road grade on each domain approach, we assume a driving cycle with varying road grades [16], [30]. However, because we could not obtain the corresponding data from a web-based search, we decided to exploit the road grade of the US12 (Fig. 2 (b)) highway as the corresponding road grade to the HWFET. Note that we have upsampled the original HWFET to have a rate of 5 Hz so that discrete dynamics can describe the vehicle motion precisely.

Both MPC frameworks require individual driving cycles defined in each domain. Fig. 3 shows time interval, δt, versus the distance traveled according to the different sampling distances. The sampling distance, Δs, is set to 4.5 meters to retain a similar sampling time to 0.2 second (5 Hz).

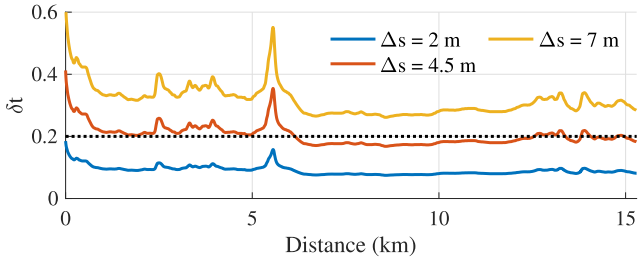

FIGURE 3. Time interval profiles of the HWFET according for three different sampling distances.

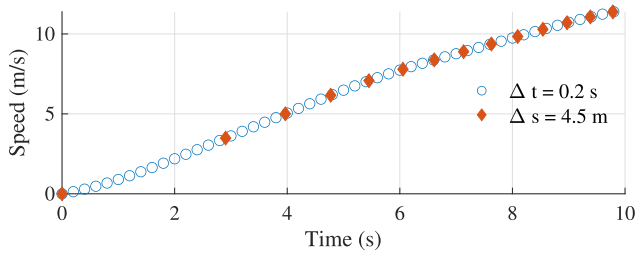

FIGURE 4. Sampling rate of each domain approach in the low-speed region of the HWFET.

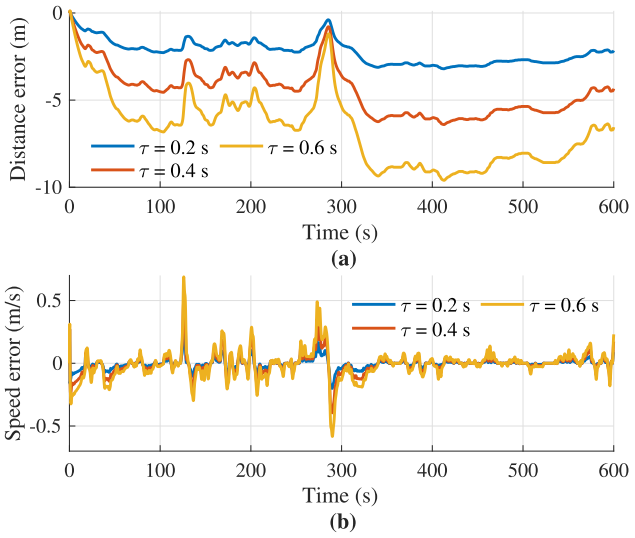

FIGURE 5. The effect of the time delay, τ, on vehicle dynamic behavior. (a) Distance error depending on various delays. (b) Speed error depending on various delays.

Fig. 4 demonstrates the reason why the space-domain model does not fit to a low-speed driving cycle. The blue dots are the upsampled HWFET data, and the red diamonds are the driving cycle for the space-domain model with a sampling distance of 4.5 meters. In contrast to the time-based data points, the number of space-based data points for the first 6 seconds is only six, which indicates that the space-domain model cannot be used for aggressive driving unless a variable sampling distance is adopted.

B. SIMULATION ASSUMPTIONS

Simulation assumptions are as follows [14]:

1) The ego vehicle knows the preceding vehicle's future status, such as speed, elapsed time, and distance traveled through V2V communication.
2) Only the forward longitudinal motion is considered.
3) There is no time delay in the ego vehicle's dynamics.

In general, the time delay includes actuator delay, communication delay, computing delay, and sensor delay [54]. In order to justify the no-delay assumption, we analyze the effect of the time delay on vehicle behavior based on the discrete second-order dynamics model [18], [45],

$$a_{i+1} = \left(1 - \frac{\Delta t}{\tau}\right) a_i + \frac{\Delta t}{\tau} a_{des,i}. \tag{9}$$

Furthermore, a discrete time delay, $D = \tau/\Delta t = 3$, which is obtained based on controller parameters, internal stability, and string stability, is adopted [55]. Simulation results in Fig. 5 confirm that distance/speed errors caused by the time delay can be bounded by certain values. The RMS distance error of the worst case, $\tau = 0.6$ s, is about 7 meters, which is within the safety distance margin for a time headway of 2 seconds. Therefore, we ignore the time delay in our study.

Instead of the dichotomous assumption that only the space-domain approach can access the road information, we divide availability of the road grade into three levels to evaluate the impact of road grade on the car-following performance in both approaches:

1) Full information on the road grade: the exact value of the road grade at every instant is available within the prediction horizon regardless of which domain is adopted.
2) Partial information on the road grade: only the road grade at the first instant in the prediction horizon is available so that the rest of the road grade is assumed to be identical to the road grade of the first instant.
3) No information on the road grade: road grade is not available; a flat road is assumed during the prediction.

The same initial condition should be provided regardless of which domain is adopted so that the simulations can be fairly compared. The ego vehicle's initial speed is set to be the same as the preceding vehicle's in both domains, $v(t_0) = v^p(t_0)$ and $v(s_0) = v^p(s_0)$. In order to satisfy the inter-vehicle distance constraints from the beginning, two vehicles are initially separated, either temporally or spatially. For the time-domain approach, the initial time headway between the ego and the preceding vehicle is set as the lower bound of the time headway,

$$s^p_{i=1} = s(t_0) + v^p(t_0) \times t^h_l. \tag{10}$$

On the other hand, for the space-domain framework, it is assumed that the ego vehicle leaves a few seconds after the departure of the preceding vehicle,

$$t_0 = t^p_{j=1} + t^h_l. \tag{11}$$

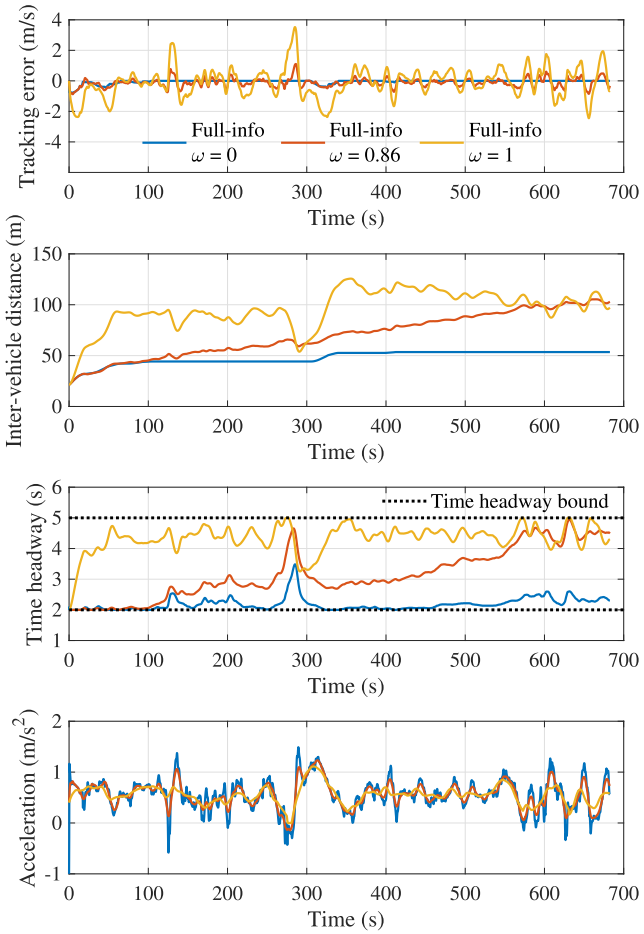

FIGURE 6. The effect of the weighting parameter, ω, on the car-following performance of using the time-domain approach when the road grade is fully given.

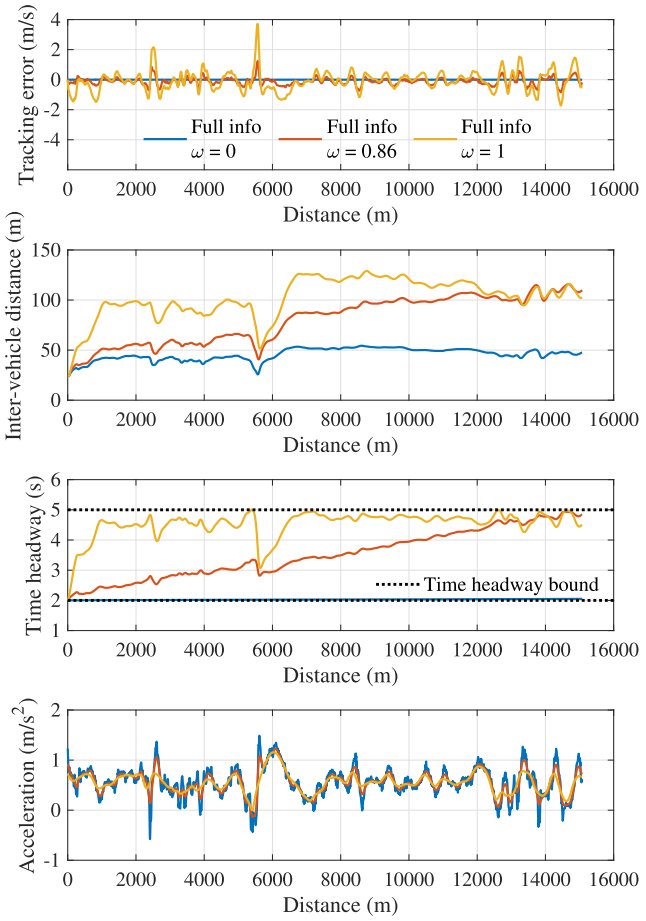

FIGURE 7. The effect of the weighting parameter, ω, on the car-following performance using the space-domain approach when the road grade is fully given.

Physically, (10) and (11) are representing the same initial condition regardless of which domain is adopted.

C. SIMULATION RESULTS: INDIVIDUAL TRAJECTORY

This section presents the ego vehicle's trajectories generated using the MPC frameworks. To analyze the performance difference between the two approaches, the availability of the road grade, and the relative weighting of the bi-objective function vary from run to run.

Figs. 6 and 7 show how the following vehicle's trajectory changes according to the various weighting parameters, ω. The ego vehicle is assumed to know the exact road grade over the prediction horizon in both cases. The first common tendency is that as the weighting parameter increases, meaning that minimizing required acceleration is more weighted than minimizing the speed-tracking errors, speed tracking error and average time headway are getting larger. Accordingly, the ego vehicle drifts away from the preceding vehicle until it reaches the maximum allowable distance such that the time headway profile almost reaches the upper bound. Since the slack variable, α, alleviates the upper bound of the time headway, occasions exceeding five seconds do not cause a constraint violation.

Significant differences in trends of the inter-vehicle distance and the time headway histories can be found in comparing between the second and fourth rows in Figs. 6 and 7. The time headway profiles of the space-domain approach tend to be more regulated than those of the time-domain approach. This phenomenon is attributed to either direct or indirect implementation of the inter-vehicle distance as suggested in (7e) and (8e). The space-domain model computes and saves the elapsed time at every instant so that it can directly use the time information to satisfy the time headway boundary. In contrast, if time is the independent variable, the time headway boundary cannot be implemented directly, so it needs to be converted into the distance traveled to constrain the inter-vehicle distance. Consequently, the time headway and inter-vehicle distance are better constrained by the space-domain and time-domain approaches, respectively.

The trajectories generated by intermediate weighting parameters (red lines) are located in between extreme cases (blue and yellow lines) in Figs. 6 and 7. Note that the intermediate weighting parameter (red lines) for each MPC

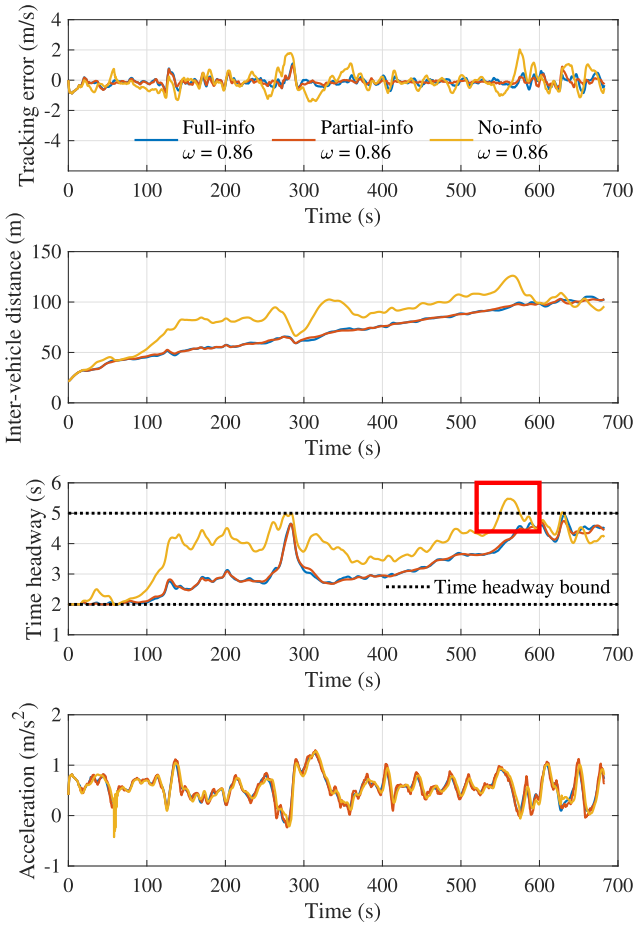

FIGURE 8. The effect of the road grade information on the car-following performance of time-domain approach when the weighting parameters, $\omega = 0.86$.

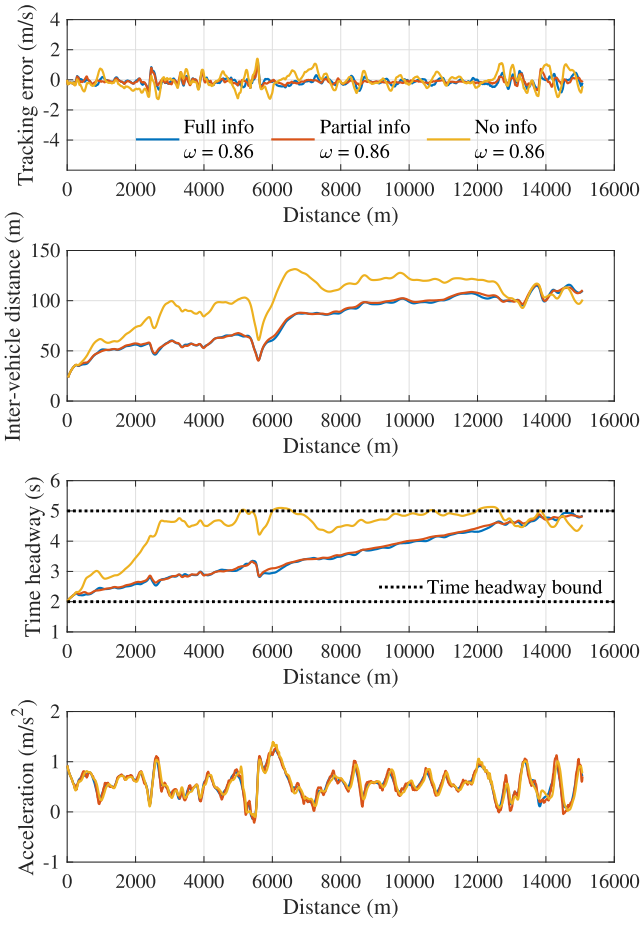

FIGURE 9. The effect of the road grade information on the car-following performance of space-domain approach when the weighting parameters, $\omega = 0.86$.

framework is the minimum value that touches the upper bound of the time headway history. Table 2 summarizes the car-following performance of each domain approach quantitatively depending on the operation type. RMS(v_{err}), $\sum FC$, $\mu(t^h)$, and $\sigma(t^h)$ are the RMS value of speed tracking error, total fuel consumption, average time headway, and standard deviation of time headway, respectively. The RMS speed errors in all three cases have a lower value in the space-domain approach. Accordingly, the fuel consumption is slightly better in the time-domain approach, but not significantly.

The effect of road grade information on the car-following performance is shown in Figs. 8 and 9. The intermediate weighting parameter of 0.86 from the red lines in Figs. 6 and 7 is selected for this experiment; thus, the blue lines in Figs. 8 and 9 are identical to the red lines in Figs. 6 and 7. We deduce that if the intermediate weighting parameter has the trajectory to barely satisfy the upper bound of time headway in the full road grade information condition, it could break the upper bound with limited information on the road grade. The time headway upper bound is exceeded in the no road grade information condition, indicated in the red rectangular box in the third row in Fig. 8. In contrast, a similar incident does not happen in the space-domain approach, and this is because the space-domain approach directly constrains the time headway between the vehicles such that the time headway history barely breaks the given threshold.

Another observation from Figs. 8 and 9 is that there is no noticeable difference between the trajectories generated by the full and partial information conditions. This phenomenon happens because the relative heavy weighting on the tracking error makes MPC less affected by the model prediction that is accomplished using the road grade information. More speculation about the relation between the tracking performance and road grade availability will be provided and examined using Pareto analysis in the following section. Table 3 summarizes the car-following performance of each domain approach quantitatively depending on the road grade information level.

D. SIMULATION RESULTS: PARETO OPTIMALITY

In this section, the optimal solutions' macroscopic trend depending on the relative weighting is examined by exploiting the concept of Pareto optimality. More specifically, the

TABLE 2. Overview of simulation results using the three different weighting parameters for each approach.

Operation type	Car-following performance	Time-domain approach	Space-domain approach
Speed tracking error minimization -oriented, $\omega = 0$	RMS(v_{err})	0.135 m/s	0.00243 m/s
	$\sum FC$	0.810 L	0.812 L
	$\mu(t^h)$	2.19 s	2.03 s
	$\sigma(t^h)$	0.210 s	0.0132 s
Intermediate, $\omega = 0.86$	RMS(v_{err})	0.296 m/s	0.271 m/s
	$\sum FC$	0.797 L	0.802 L
	$\mu(t^h)$	3.17 s	3.52 s
	$\sigma(t^h)$	0.810 s	0.796 s
Acceleration minimization -oriented, $\omega = 1$	RMS(v_{err})	0.970 m/s	0.674 m/s
	$\sum FC$	0.790 L	0.796 L
	$\mu(t^h)$	4.35 s	4.54 s
	$\sigma(t^h)$	0.419 s	0.422 s

TABLE 3. Overview of simulation results using the three different road grade information levels for the time-domain and the space-domain approaches.

Road grade cases	Car-following performance	Time-domain approach	Space-domain approach
Full information	RMS(v_{err})	0.296 m/s	0.271 m/s
	$\sum FC$	0.797 L	0.802 L
	$\mu(t^h)$	3.168 s	3.52 s
	$\sigma(t^h)$	0.810 s	0.796 s
Partial information	RMS(v_{err})	0.249 m/s	0.216 m/s
	$\sum FC$	0.802 L	0.806 L
	$\mu(t^h)$	3.168 s	3.55 s
	$\sigma(t^h)$	0.798s	0.797 s
No information (Flat road assumed)	RMS(v_{err})	0.615 m/s	0.485 m/s
	$\sum FC$	0.795 L	0.804 L
	$\mu(t^h)$	3.84 s	4.44 s
	$\sigma(t^h)$	0.842 s	0.709 s

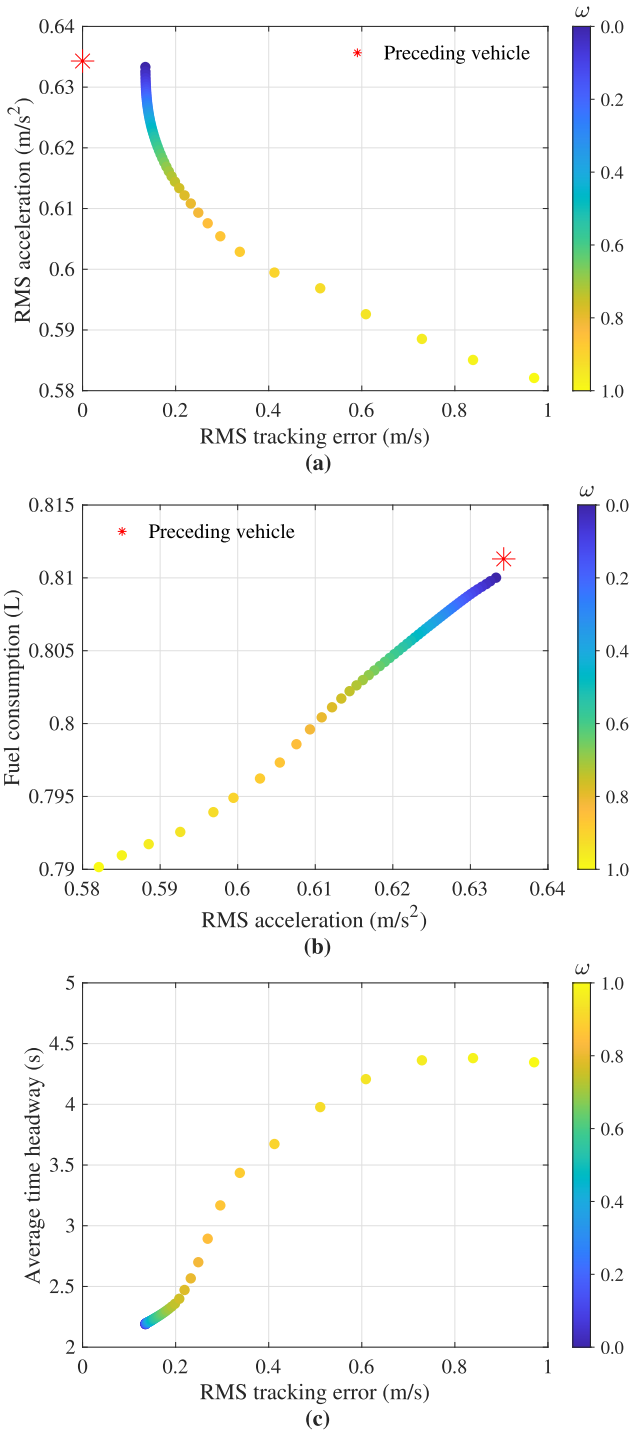

FIGURE 10. A 51-run simulation using the time-domain MPC framework when the weighting parameter ω on a^2_{des} increases from 0 to 1, and the true road grade is available. (a) Pareto front showing the trade-off in the bi-objective cost function, (b) A near-linear relationship between desired acceleration and fuel consumption, (c) The correlation between RMS speed tracking error and time headway.

bi-objective cost function is designed to minimize the speed tracking error and the desired acceleration. The conflicting relationship between them is revealed through changing the weighting parameter, ω, linearly from 0 to 1.

Fig. 10 displays the simulation results of the time-domain approach when the true road grade is available. The red asterisk indicates a backward propagation result of the HWFET, which is assumed as the driving cycle of the preceding vehicle. The required acceleration and fuel consumption of the HWFET are computed based on the vehicle dynamics models, (1) and (4), and the fuel consumption model, (6), respectively. The gap between the red asterisk and the leftmost

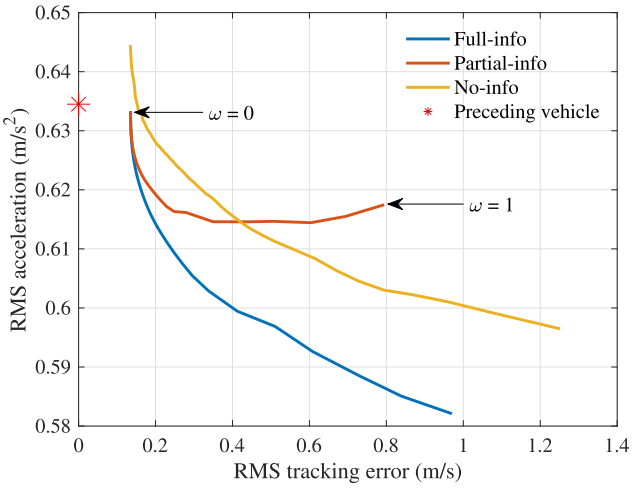

FIGURE 11. Pareto fronts of the time-domain MPC framework with three levels of the road grade availability.

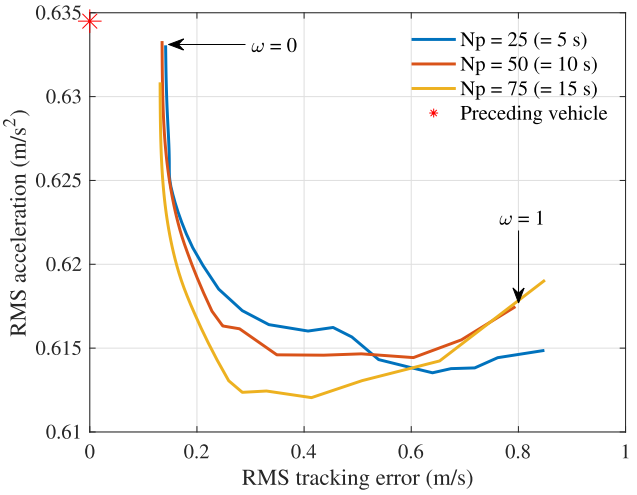

FIGURE 12. Pareto analysis of the time-domain approach showing the effects of the prediction horizon length on partial information case.

point ($\omega = 0$) of the Pareto front is inevitable due to the safety distance, which is given as the lower bound of the time headway. Fig. 10 (a) demonstrates the fact that one objective cannot be improved without deteriorating the other. On ther other hand, Fig. 10 (b) justifies the cost function design in (7a) and (8a). Since a near-linear relationship exists between the quadratic acceleration term and fuel consumption, the a^2 term can replace an elaborate fuel consumption model, so we keep using RMS acceleration as a fuel consumption indicator throughout this section. Fig. 10 (c) reveals another relationship between time headway and speed tracking error, which means that adverse tracking performance results in the ego vehicle drifting away from the preceding vehicle.

Fig. 11 shows the impact of road grade availability on the performance of the time-domain MPC framework. Note that the solid blue line in Fig. 11 is identical to the one at Fig. 10 (a).

The partial information case's Pareto front starts from the same point as the full information case, and its RMS acceleration stops decreasing when it reaches about 0.615 m/s^2. The first phenomenon is attributed to three factors: 1) the first instant's road grade in the partial information case is identical to the one in the full information case, 2) the prediction horizon is receding every one step, and 3) in the case of the tracking error minimization-oriented operation, the solver focuses more on the tracking rather than reducing the desired acceleration. Consequently, the partial information and the full information cases produce the same performance. On the other hand, when the weighting parameter increases, the solver places more reliance on the road information to reduce the desired acceleration. As a result, no improvement in RMS acceleration can be achieved with the limited information on the road grade; instead, the RMS speed tracking error deteriorates as the weighting on the desired acceleration increases. Fig. 12 supports the reason for such behavior in the partial information case. The longer the prediction horizon, the more incorrect road data will be used to predict the vehicle motion, resulting in inefficient fuel/energy consumption

The no information case requires more desired acceleration than the full information case to achieve the same speed tracking performance. This is because the solver calculates the desired acceleration without knowing the road grade. However, it can be noticed that the no information case can achieve a smaller RMS acceleration than the partial information case when higher weighting on the desired acceleration is imposed. This means that if one wants to minimize the desired acceleration using an MPC-based algorithm, the flat road assumption can be a better option than providing the wrong road information throughout the prediction horizon except for the first step.

Likewise, Fig. 13 presents the optimal solution's macroscopic trends in the space-domain MPC framework. The overall tendencies of Figs. 10 and 13 are similar to each other, but there are a few notable differences between them. First, the minimum and maximum RMS speed tracking error of the space-domain approach is smaller than that of the time-domain approach. Unlike the time-domain approach, the minimum average time headway of the space-domain approach touches the lower boundary, as shown in the individual trajectory plots in Fig. 7. Consequently, the space-domain approach can achieve the same performance as the preceding vehicle for the minimum tracking error operation. This phenomenon occurs due to the difference in the way of constraining the inter-vehicle distance between the two approaches. On the other hand, there is no significant difference in fuel consumption.

Fig. 14 illustrates the Pareto fronts in the space-domain approach that differ depending on the road grade cases. Comparing Figs. 11 and 14, it is observed that both approaches share several features in common. The costs in the bi-objective function conflict with each other, the partial information case has a higher limit in the RMS acceleration,

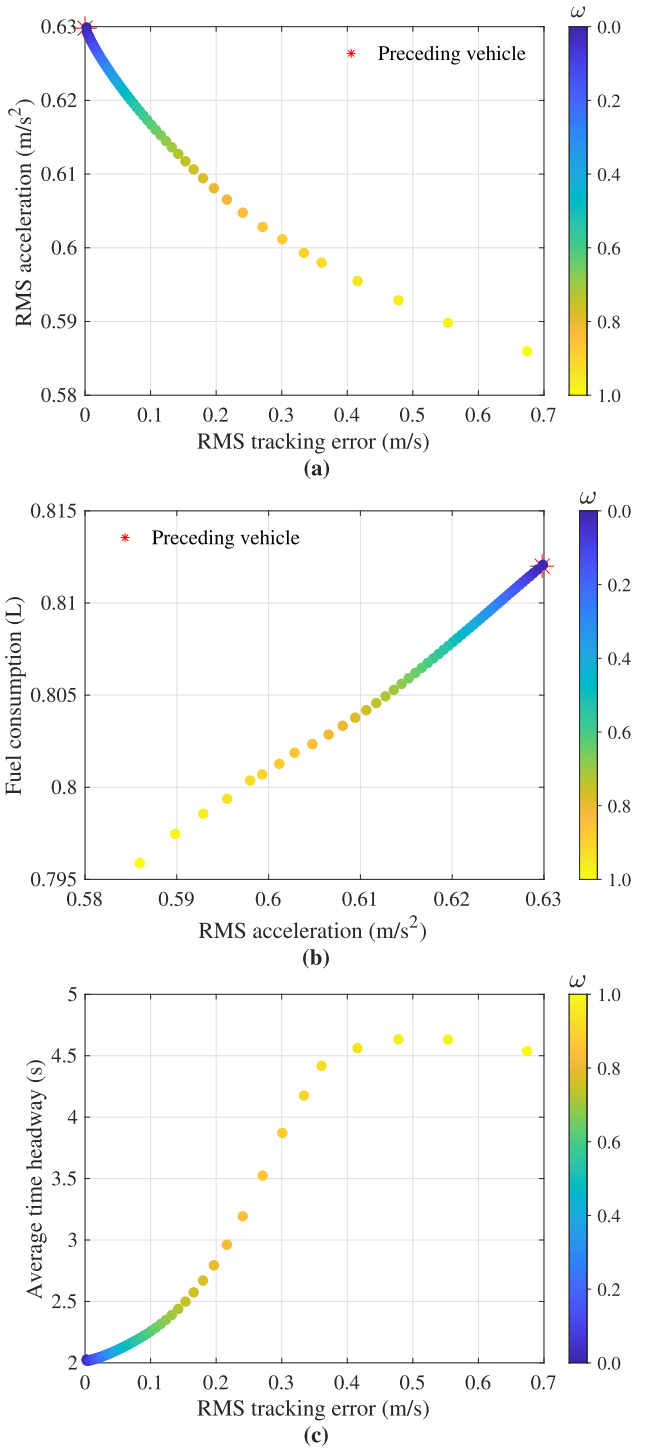

FIGURE 13. A 51-run simulation using the space-domain MPC framework when the weighting parameter ω on a^2_{des} increases from 0 to 1, and the true road grade is available. (a) Pareto front showing the trade-off in the bi-objective cost function, (b) A near-linear relationship between desired acceleration and fuel consumption, (c) The correlation between RMS speed tracking error and time headway.

and the space-domain MPC framework without road grade information can produce better fuel-efficient driving than in the partial information condition. However, there exist a few

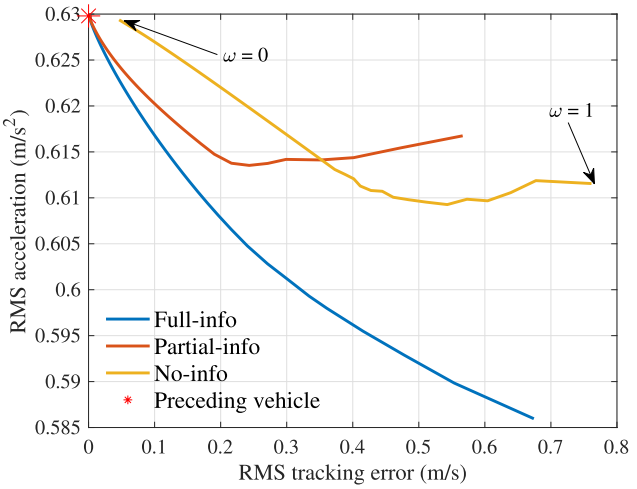

FIGURE 14. Pareto fronts of the space-domain MPC framework with three levels of road grade availability.

differences as well. Unlike the no-grade information case in the time-domain approach, the one in the space-domain approach 1) does not exceed the RMS acceleration value of the preceding vehicle, and 2) has a lower bound in terms of RMS acceleration of around 0.61 m/s^2.

To elaborate on this phenomenon from the viewpoint of speed tracking error, the near-linear relationship between tracking error and time headway that is revealed from Figs. 10 and 13 is used. Figs. 15 and 16 display the time headway histories of two extreme cases that differentiate themselves from the others depending on the adopted domain, weighting parameter, and road grade condition. When $\omega = 1$, the time headway profile of the no information case in the time-domain approach repeatedly crosses the upper bound while that of the space-domain approach is well managed within the upper boundary.

Table 4 summarizes the simulation results shown in Figs. 15 and 16. One can notice that the time headway histories of the space-domain approach achieve significantly low standard deviations compared with the time-domain approach when $\omega = 0$. In the case of $\omega = 1$, the standard deviation of the space-domain approach is 36% smaller than that of the time-domain approach.

E. PARETO ANALYSIS

In order to quantitatively assess the Pareto fronts of each approach, we exploit the concept of utopia point (UP). The utopia point is obtained by optimizing all individual objectives in a multi-objective cost function separately [56]–[58]. Because all individual objectives cannot be minimized simultaneously and independently, the utopia point is unattainable and does not belong to the Pareto front. Instead, one can find the closest point from the utopia point to a feasible optimal solution on the Pareto front, which is called a compromised solution (CS).

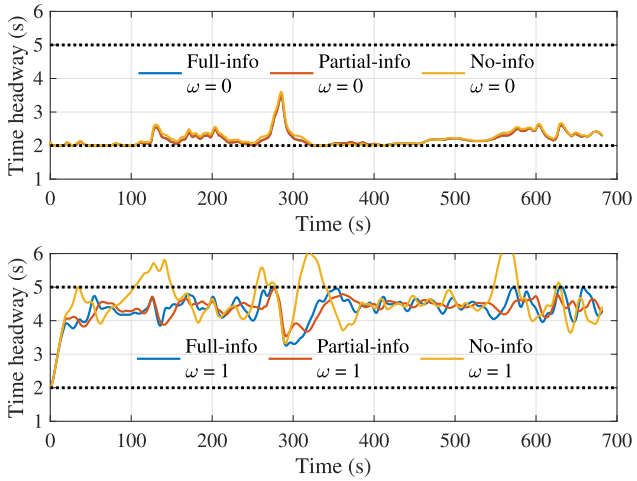

FIGURE 15. Time headway histories of two extreme cases using the time-domain approach.

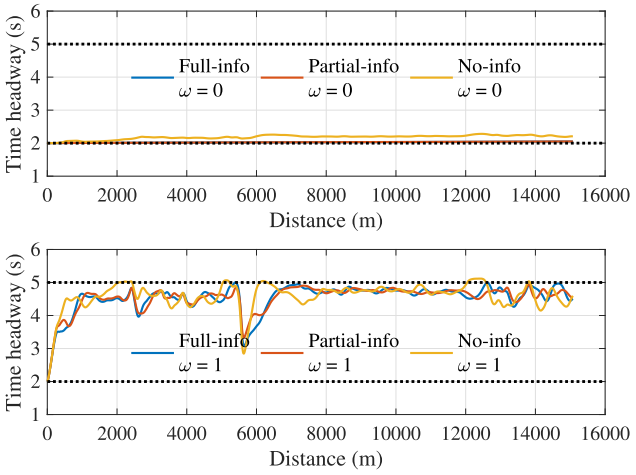

FIGURE 16. Time headway histories of two extreme cases using the space-domain approach.

TABLE 4. Overview of each simulation's time headway history according to different domains, weighting parameters, and road grade cases.

Operation type	Road grade cases	Car-following performance	Time-domain approach	Space-domain approach
Speed tracking error minimization -oriented, $\omega = 0$	Full -info	$\mu(t^h)$	2.19 s	2.03 s
		$\sigma(t^h)$	0.210 s	0.0132 s
	Partial -info	$\mu(t^h)$	2.19 s	2.03 s
		$\sigma(t^h)$	0.210 s	0.0137 s
	No -info	$\mu(t^h)$	2.22 s	2.18 s
		$\sigma(t^h)$	0.234 s	0.0624 s
Acceleration minimization -oriented, $\omega = 1$	Full -info	$\mu(t^h)$	4.35 s	4.54 s
		$\sigma(t^h)$	0.419 s	0.422 s
	Partial -info	$\mu(t^h)$	4.35 s	4.54 s
		$\sigma(t^h)$	0.352 s	0.375 s
	No -info	$\mu(t^h)$	4.58 s	4.59 s
		$\sigma(t^h)$	0.629 s	0.400 s

Let $J_{1,min}$ and $J_{2,min}$ be the minimum values of each objective in our bi-objective cost functions, (7a) and (8a). Then, the utopia point is found as

$$UP = \left(J_{1,min}, J_{2,min}\right), \tag{12}$$

and the Euclidean distance from the utopia point to lth optimal solution can be computed in the sense of 2-norm [56], [57].

$$D_l = \| \left(J_1^l, J_2^l\right) - \left(J_{1,min}, J_{2,min}\right) \| \tag{13}$$

where $l = 1, 2, \cdots, N$. An optimal solution with the minimum D becomes the compromised solution. The utopia point implies a feasible lower boundary that an operation can achieve, and the compromised solution indicates the well-balanced feasible solution of the problem.

TABLE 5. Overview of Pareto fronts assessment that shows the utopia point, compromised solution, and optimal weighting parameter according to road grade availability and domain adopted.

Road grade cases	Pareto front assessment		Time-domain approach	Space-domain approach
Full information	UP	RMS(v_{err})	0.135 m/s	0.002434 m/s
		RMS(a_{des})	0.582 m/s^2	0.586 m/s^2
	CS	RMS(v_{err})	0.149 m/s	0.0094 m/s
		RMS(a_{des})	0.623 m/s^2	0.628 m/s^2
		ω_{CS}	0.46	0.08
Partial information	UP	RMS(v_{err})	0.135 m/s	0.00245 m/s
		RMS(a_{des})	0.614 m/s^2	0.614 m/s^2
	CS	RMS(v_{err})	0.140 m/s	0.00443 m/s
		RMS(a_{des})	0.627 m/s^2	0.629 m/s^2
		ω_{CS}	0.36	0.04
No information (Flat road assumed)	UP	RMS(v_{err})	0.134 m/s	0.0463 m/s
		RMS(a_{des})	0.597 m/s^2	0.609 m/s^2
	CS	RMS(v_{err})	0.148 m/s	0.04631 m/s
		RMS(a_{des})	0.636 m/s^2	0.629 m/s^2
		ω_{CS}	0.08	0

Table 5 summarizes the Pareto fronts assessment. The compromised solutions of the space-domain approach are slightly better those of the time-domain approach. Especially, the more limited road grade we have, the lower the ω value of the CS. This means that achieving fuel-efficient driving is a challenging task without road grade information.

V. DISCUSSION

This section summarizes and discusses the results obtained in this paper. The time and space-domain MPC frameworks demonstrate satisfactory performance in that they can achieve either fuel-efficient or minimum tracking error trajectories while satisfying the inter-vehicle distance constraints. Regardless of the adopted domain, the simple quadratic acceleration term shows a linear relationship with fuel consumption as displayed in the second row of Figs. 10 and 13, so it can replace the complex fuel consumption model and reduce the computation time.

The two types of MPC frameworks show different performances depending on how car-following constraints are set. An important difference between the models comes from whether they are linear or nonlinear. The linearity in the time-domain vehicle dynamics model brings a computational advantage. The time-domain MPC framework takes about 0.19 seconds to compute each step. In contrast, the nonlinearity in the space-domain vehicle dynamics model requires additional computation such that it takes about 0.22 seconds for the computation of each step, which is 14% higher than the time-domain approach.

A. FEATURES OF THE TIME-DOMAIN APPROACH

We assume that the time-domain vehicle dynamics model can predict only with current road grade information for practical reasons. The performance of MPC with such partial information is compared to the cases with no and full grade information.

- In the case of minimizing the tracking error, it shows similar performance whether the road information is fully or partially provided. The blue and red lines in the second rows of Figs. 8 and 11 prove this phenomenon.
- In the case of partial road information, even with the increased weight on the acceleration term, at some weighting point, the fuel efficiency cannot be improved anymore, and the tracking performance starts to deteriorate. This is shown by the red line of Fig. 11.
- This also proves that prediction with inaccurate information can even deteriorate the performance of the MPC-based algorithm. In the same vein, a longer prediction horizon does not guarantee improved fuel efficiency, or rather, the longer prediction horizon can even deteriorate fuel efficiency, which is presented in Fig. 12.
- Model prediction assuming a flat road can be a better option for achieving fuel-efficient driving compared to the partial road grade assumption, as demonstrated in Fig. 11.

B. FEATURES OF THE SPACE-DOMAIN APPROACH

Several notable aspects in the space-domain approach are observed as follows.

- The space-domain approach has better time headway tracking performance than the time-domain approach, as illustrated in Figs. 7 and 16, and compared in Table 4.
- If the MPC framework is solely focusing on tracking performance without considering fuel efficiency, the time headway can achieve the lower limit of the inter-vehicle distance constraint, which is supported by the low RMS tracking error in Table 5.

In summary, we conclude that one should consider the application's purpose and available information before selecting either the time-domain or the space-domain vehicle models. First, for applications that aim to maintain a constant inter-vehicle distance between vehicles [59], [60], the time-domain approach performs better than the space-domain approach. On the other hand, if an application's purpose is maintaining a constant time headway between vehicles [61]–[63], then the space-domain approach is recommended. When an application focuses on fuel efficiency, the designer should recognize that the performance of the time-domain approach is greatly affected by the road grade information. Even though this tendency is also true in the space-domain approach, we do not have to worry about it due to easy access to road information. Lastly, suppose the application wants to minimize speed-tracking errors. In that case, a space-domain approach can be a better solution than a time-domain approach regardless of the road grade information level.

VI. CONCLUSION

This paper present the distinctions between two MPC frameworks based on the time-domain and space-domain vehicle models for autonomous highway driving. The design process and analysis method are suggested and demonstrated for equivalent performance comparison. In order to analyze trends between speed tracking and fuel-saving performance, which are conflicting car-following objectives, a bi-objective cost function is proposed and manipulated by varying the weighting parameter. It is found that the space-domain approach presents stable tracking performance, and the time-domain approach shows better fuel efficiency. However, the space-domain approach utilizing road information excels in tracking and fuel efficiency compared to the time-domain model with limited road information. Pareto analysis was conducted to visualize and describe performance differences in various situations regarding tracking error, fuel efficiency, and road grade information levels. Based on the results, a selection strategy for the domain is proposed in developing an MPC-based algorithm for car-following problems with inter-vehicle distance constraints.

REFERENCES

[1] L.-H. Luo, H. Liu, P. Li, and H. Wang, "Model predictive control for adaptive cruise control with multi-objectives: Comfort, fuel-economy, safety and car-following," *J. Zhejiang Univ. Sci. A*, vol. 11, no. 3, pp. 191–201, Mar. 2010.

[2] Y. Jia, T. Saito, Y. Itoh, Y. Nukezhanov, and D. Görges, "Energy-optimal adaptive cruise control in time domain based on model predictive control," *IFAC-PapersOnLine*, vol. 51, no. 31, pp. 846–853, 2018.

[3] T. Takahama and D. Akasaka, "Model predictive control approach to design practical adaptive cruise control for traffic jam," *Int. J. Automot. Eng.*, vol. 9, no. 3, pp. 99–104, 2018.

[4] M. A. S. Kamal, M. Mukai, J. Murata, and T. Kawabe, "Ecological driver assistance system using model-based anticipation of vehicle–road–traffic information," *IET Intell. Transp. Syst.*, vol. 4, no. 4, p. 244, 2010.
[5] C. R. He, A. Alan, T. G. Molnar, S. S. Avedisov, A. H. Bell, R. Zukouski, M. Hunkler, J. Yan, and G. Orosz, "Improving fuel economy of heavy-duty vehicles in daily driving," in *Proc. Amer. Control Conf. (ACC)*, Jul. 2020, pp. 2306–2311.
[6] H. Xiao, Y. Chen, S. Ouyang, and A. T. Chronopoulos, "Power control for clustering car-following V2X communication system with non-orthogonal multiple access," *IEEE Access*, vol. 7, pp. 68160–68171, 2019.
[7] T. Stanger and L. del Re, "A model predictive cooperative adaptive cruise control approach," in *Proc. Amer. Control Conf.*, Jun. 2013, pp. 1374–1379.
[8] M. A. S. Kamal, M. Mukai, J. Murata, and T. Kawabe, "Model predictive control of vehicles on urban roads for improved fuel economy," *IEEE Trans. Control Syst. Technol.*, vol. 21, no. 3, pp. 831–841, May 2013.
[9] B. Asadi and A. Vahidi, "Predictive cruise control: Utilizing upcoming traffic signal information for improving fuel economy and reducing trip time," *IEEE Trans. Control Syst. Technol.*, vol. 19, no. 3, pp. 707–714, May 2011.
[10] E. Hellström, J. Åslund, and L. Nielsen, "Design of an efficient algorithm for fuel-optimal look-ahead control," *Control Eng. Pract.*, vol. 18, no. 11, pp. 1318–1327, Nov. 2010.
[11] E. Hyeon, Y. Kim, N. Prakash, and A. G. Stefanopoulou, "Short-term speed forecasting using vehicle wireless communications," in *Proc. Amer. Control Conf. (ACC)*, Jul. 2019, pp. 736–741.
[12] S. Li, K. Li, R. Rajamani, and J. Wang, "Model predictive multi-objective vehicular adaptive cruise control," *IEEE Trans. Control Syst. Technol.*, vol. 19, no. 3, pp. 556–566, May 2011.
[13] D. Lang, T. Stanger, and L. del Re, "Opportunities on fuel economy utilizing V2V based drive systems," in *Proc. SAE Tech. Paper Ser.*, Apr. 2013, pp. 1–7.
[14] Y. He, Y. Kim, D. Y. Lee, and S.-H. Kim, "Defensive ecological adaptive cruise control considering neighboring Vehicles' blind-spot zones," *IEEE Access*, vol. 9, pp. 152275–152287, 2021. [Online]. Available: https://ieeexplore.ieee.org/document/9611213/
[15] X. Chen, J. Yang, C. Zhai, J. Lou, and C. Yan, "Economic adaptive cruise control for electric vehicles based on ADHDP in a car-following scenario," *IEEE Access*, vol. 9, pp. 74949–74958, 2021.
[16] C. Zhai, F. Luo, Y. Liu, and Z. Chen, "Ecological cooperative look-ahead control for automated vehicles travelling on freeways with varying slopes," *IEEE Trans. Veh. Technol.*, vol. 68, no. 2, pp. 1208–1221, Feb. 2019.
[17] V. Turri, Y. Kim, J. Guanetti, K. H. Johansson, and F. Borrelli, "A model predictive controller for non-cooperative eco-platooning," in *Proc. Amer. Control Conf. (ACC)*, May 2017, pp. 2309–2314.
[18] L. Guo, P. Ge, Y. Qiao, and L. Xu, "Multi-objective adaptive cruise control strategy based on variable time headway," in *Proc. IEEE Intell. Vehicles Symp. (IV)*, Jun. 2018, pp. 203–208.
[19] L. Bertoni, J. Guanetti, M. Basso, M. Masoero, S. Cetinkunt, and F. Borrelli, "An adaptive cruise control for connected energy-saving electric vehicles," *IFAC-PapersOnLine*, vol. 50, no. 1, pp. 2359–2364, Jul. 2017.
[20] Z. Pu, X. Jiao, C. Yang, and S. Fang, "An adaptive stochastic model predictive control strategy for plug-in hybrid electric bus during vehicle-following scenario," *IEEE Access*, vol. 8, pp. 13887–13897, 2020.
[21] A. Lelouvier, J. Guanetti, and F. Borrelli, "Eco-platooning of autonomous electrical vehicles using distributed model predictive control," in *Proc. IEEE 20th Intell. Transp. Syst. Conf.*, Jul. 2017, pp. 1–10.
[22] Q. Zhou, D. Zhao, B. Shuai, Y. Li, H. Williams, and H. Xu, "Knowledge implementation and transfer with an adaptive learning network for real-time power management of the plug-in hybrid vehicle," *IEEE Trans. Neural Netw. Learn. Syst.*, early access, Jul. 14, 2021, doi: 10.1109/TNNLS.2021.3093429.
[23] M. Barth, G. Scora, and T. Younglove, "Modal emissions model for heavy-duty diesel vehicles," *Transp. Res. Rec., J. Transp. Res. Board*, vol. 1880, no. 1, pp. 10–20, Jan. 2004.
[24] F. Morlock, U. Wohlhaupter, and O. Sawodny, "Real-time capable driving strategy for EVs using linear MPC," in *Proc. Amer. Control Conf. (ACC)*, Jul. 2019, pp. 304–309.
[25] S. Xu and H. Peng, "Design and comparison of fuel-saving speed planning algorithms for automated vehicles," *IEEE Access*, vol. 6, pp. 9070–9080, 2018.
[26] T. Schwickart, H. Voos, and M. Darouach, "A real-time implementable model-predictive cruise controller for electric vehicles and energy-efficient driving," in *Proc. IEEE Conf. Control Appl. (CCA)*, Oct. 2014, pp. 617–622.
[27] A. Fröberg and L. Nielsen, "Optimal fuel and gear ratio control for heavy trucks with piece wise affine engine characteristics," *IFAC Proc. Volumes*, vol. 40, no. 10, pp. 335–342, 2007.
[28] C. R. He, J. I. Ge, and G. Orosz, "Fuel efficient connected cruise control for heavy-duty trucks in real traffic," *IEEE Trans. Control Syst. Technol.*, vol. 28, no. 6, pp. 2474–2481, Nov. 2020.
[29] H. Chu, L. Guo, H. Chen, and B. Gao, "Optimal car-following control for intelligent vehicles using online road-slope approximation method," *Sci. China Inf. Sci.*, vol. 64, no. 1, pp. 1–16, Jan. 2021.
[30] C. Zhai, F. Luo, and Y. Liu, "Cooperative power split optimization for a group of intelligent electric vehicles travelling on a highway with varying slopes," *IEEE Trans. Intell. Transp. Syst.*, early access, Dec. 29, 2021, doi: 10.1109/TITS.2020.3045264.
[31] N. Murgovski and J. Sjoberg, "Predictive cruise control with autonomous overtaking," in *Proc. 54th IEEE Conf. Decis. Control (CDC)*, Dec. 2015, pp. 644–649. [Online]. Available: http://ieeexplore.ieee.org/document/7402302/
[32] M. Graf Plessen, D. Bernardini, H. Esen, and A. Bemporad, "Spatial-based predictive control and geometric corridor planning for adaptive cruise control coupled with obstacle avoidance," *IEEE Trans. Control Syst. Technol.*, vol. 26, no. 1, pp. 38–50, Jan. 2018.
[33] L. Zhang, F. Chen, X. Ma, and X. Pan, "Fuel economy in truck platooning: A literature overview and directions for future research," *J. Adv. Transp.*, vol. 2020, pp. 1–10, 2020.
[34] B. HomChaudhuri, A. Vahidi, and P. Pisu, "Fast model predictive control-based fuel efficient control strategy for a group of connected vehicles in urban road conditions," *IEEE Trans. Control Syst. Technol.*, vol. 25, no. 2, pp. 760–767, Mar. 2017.
[35] X. Hu, H. Wang, and X. Tang, "Cyber-physical control for energy-saving vehicle following with connectivity," *IEEE Trans. Ind. Electron.*, vol. 64, no. 11, pp. 8578–8587, Nov. 2017.
[36] M. F. Ozkan and Y. Ma, "A predictive control design with speed previewing information for vehicle fuel efficiency improvement," in *Proc. Amer. Control Conf. (ACC)*, Jul. 2020, pp. 2312–2317.
[37] M. Rodriguez and H. Fathy, "Speed trajectory optimization for a heavy-duty truck traversing multiple signalized intersections: A dynamic programming study," in *Proc. IEEE Conf. Control Technol. Appl. (CCTA)*, Aug. 2018, pp. 1454–1459.
[38] X. Hu, Y. Li, C. Lv, and Y. Liu, "Optimal energy management and sizing of a dual motor-driven electric powertrain," *IEEE Trans. Power Electron.*, vol. 34, no. 8, pp. 7489–7501, Aug. 2019.
[39] S. E. Li, Z. Jia, K. Li, and B. Cheng, "Fast online computation of a model predictive controller and its application to fuel economy–oriented adaptive cruise control," *IEEE Trans. Intell. Transp. Syst.*, vol. 16, no. 3, pp. 1199–1209, Jun. 2015.
[40] L. Schmitt, M. Keller, T. Albin, and D. Abel, "Real-time nonlinear model predictive control for the energy management of hybrid electric vehicles in a hierarchical framework," in *Proc. Amer. Control Conf. (ACC)*, Jul. 2020, pp. 1961–1967.
[41] N. Gunantara, "A review of multi-objective optimization: Methods and its applications," *Cogent Eng.*, vol. 5, no. 1, Jan. 2018, Art. no. 1502242.
[42] P. P. Dey and S. Chandra, "Desired time gap and time headway in steady-state car-following on two-lane roads," *J. Transp. Eng.*, vol. 135, no. 10, pp. 687–693, Oct. 2009.
[43] E. Hyeon, Y. Kim, N. Prakash, and A. G. Stefanopoulou, "Influence of speed forecasting on the performance of ecological adaptive cruise control," in *Proc. ASME Dyn. Syst. Control Conf., (DSCC)*, vol. 1, Oct. 2019, Art. no. V001T08A003.
[44] H. Abbas, Y. Kim, J. B. Siegel, and D. M. Rizzo, "Synthesis of Pontryagin's maximum principle analysis for speed profile optimization of all-electric vehicles," *J. Dyn. Syst., Meas., Control*, vol. 141, no. 7, pp. 071004-1–071004-10, Jul. 2019.
[45] J.-Q. Wang, S. E. Li, Y. Zheng, and X.-Y. Lu, "Longitudinal collision mitigation via coordinated braking of multiple vehicles using model predictive control," *Integr. Comput.-Aided Eng.*, vol. 22, no. 2, pp. 171–185, Feb. 2015.
[46] S. Park, H. Rakha, K. Ahn, and K. Moran, "Virginia tech comprehensive power-based fuel consumption model (VT-CPFM): Model validation and calibration considerations," *Int. J. Transp. Sci. Technol.*, vol. 2, no. 4, pp. 317–336, Dec. 2013.

[47] H. A. Rakha, K. Ahn, K. Moran, B. Saerens, and E. V. D. Bulck, "Virginia tech comprehensive power-based fuel consumption model: Model development and testing," *Transp. Res. D, Transp. Environ.*, vol. 16, no. 7, pp. 492–503, Oct. 2011.
[48] E. F. Meyer, III, "Multiple-car pileups and the two-second rule," *Phys. Teacher*, vol. 32, no. 8, pp. 496–497, Nov. 1994.
[49] S. U. Sharma and D. J. Shah, "A practical animal detection and collision avoidance system using computer vision technique," *IEEE Access*, vol. 5, pp. 347–358, 2017.
[50] S. Yousif, M. Alterawi, and R. R. Henson, "Red light running and close following behaviour at urban shuttle-lane roadworks," *Accident Anal. Prevention*, vol. 66, pp. 147–157, May 2014.
[51] M. N. Zeilinger, C. N. Jones, and M. Morari, "Real-time suboptimal model predictive control using a combination of explicit MPC and online optimization," *IEEE Trans. Autom. Control*, vol. 56, no. 7, pp. 1524–1534, Jul. 2011.
[52] Y. Kim and M. Anitescu, "A real-time optimization with warm-start of multiperiod AC optimal power flows," *Electr. Power Syst. Res.*, vol. 189, Dec. 2020, Art. no. 106721.
[53] E. John and E. A. Yıldırım, "Implementation of warm-start strategies in interior-point methods for linear programming in fixed dimension," *Comput. Optim. Appl.*, vol. 41, no. 2, pp. 151–183, Nov. 2008.
[54] Y. Liu, H. Gao, C. Zhai, and W. Xie, "Internal stability and string stability of connected vehicle systems with time delays," *IEEE Trans. Intell. Transp. Syst.*, vol. 22, no. 10, pp. 6162–6174, Oct. 2021.
[55] C. Zhai, X. Chen, C. Yan, Y. Liu, and H. Li, "Ecological cooperative adaptive cruise control for a heterogeneous platoon of heavy-duty vehicles with time delays," *IEEE Access*, vol. 8, pp. 146208–146219, 2020.
[56] D. He, Y. Shi, and X. Song, "Weight-free multi-objective predictive cruise control of autonomous vehicles in integrated perturbation analysis and sequential quadratic programming optimization framework," *J. Dyn. Syst., Meas., Control*, vol. 141, no. 9, Sep. 2019, Art. no. 091015.
[57] Y. Shi, X. Song, and D. He, "Utopia-tracking multi-performance predictive cruise control for a group of connected vehicles on urban roads," in *Proc. Chin. Control Decis. Conf. (CCDC)*, Jun. 2018, pp. 1883–1888.
[58] Y. He, Q. Zhou, M. Makridis, K. Mattas, J. Li, H. Williams, and H. Xu, "Multiobjective co-optimization of cooperative adaptive cruise control and energy management strategy for PHEVs," *IEEE Trans. Transport. Electrific.*, vol. 6, no. 1, pp. 346–355, Mar. 2020.
[59] J. Smith, R. Mihelic, B. Gifford, and M. Ellis, "Aerodynamic impact of tractor-trailer in drafting configuration," *SAE Int. J. Commercial Vehicles*, vol. 7, no. 2, pp. 619–625, Sep. 2014.
[60] S. Tsugawa, S. Kato, and K. Aoki, "An automated truck platoon for energy saving," in *Proc. IEEE/RSJ Int. Conf. Intell. Robots Syst.*, Sep. 2011, pp. 4109–4114.
[61] V. Turri, B. Besselink, and K. H. Johansson, "Cooperative look-ahead control for fuel-efficient and safe heavy-duty vehicle platooning," *IEEE Trans. Control Syst. Technol.*, vol. 25, no. 1, pp. 12–28, Jan. 2017.
[62] A. Alam, J. Mårtensson, and K. H. Johansson, "Experimental evaluation of decentralized cooperative cruise control for heavy-duty vehicle platooning," *Control Eng. Pract.*, vol. 38, pp. 11–25, May 2015.
[63] T. Ard, F. Ashtiani, A. Vahidi, and H. Borhan, "Optimizing gap tracking subject to dynamic losses via connected and anticipative MPC in truck platooning," in *Proc. Amer. Control Conf. (ACC)*, Jul. 2020, pp. 2300–2305.

YOUNGRO LEE (Student Member, IEEE) received the B.S and M.S. degrees in science from Yonsei University, Seoul, South Korea, in 2016 and 2018, respectively. He is currently pursuing the Ph.D. degree in aerospace engineering with Iowa State University, Ames, IA, USA.

Since 2019, he has been working as a Research Assistant at the Cardinal Space Laboratory, Iowa State University. His research interests include optimal control of automotive vehicles and optimal guidance of spacecraft.

DAE YOUNG LEE (Member, IEEE) received the B.S. and M.S. degrees in mechanical engineering from Pusan National University, Busan, South Korea, in 1997 and 2001, respectively, and the M.S. and Ph.D. degrees in aerospace engineering from the University of Michigan, Ann Arbor, MI, USA, in 2016.

He worked as a Research Engineer at Hyundai and LG for nine years. From 2016 to 2018, he was a Postdoctoral Researcher at the Center of Space Research, The University of Texas at Austin, Austin, TX, USA. He is currently an Assistant Professor of aerospace engineering at Iowa State University, Ames, IA, USA. He is also the Director of the Cardinal Space Laboratory and researching spacecraft attitude determination and control, Mars entry, descent, landing, in-space manufacturing, and space mission development using the CubeSat platform. His research interests include non-linear model predictive control of the car, drone, and spacecraft fleet with various constraints.

SEUNG HWAN LEE (Member, IEEE) received the B.S. degree from Hanyang University, Seoul, South Korea, in 2004, and the M.S. and Ph.D. degrees in mechanical engineering from the University of Michigan, Ann Arbor, MI, USA, in 2007 and 2013, respectively.

After the graduation, he worked at Samsung Electronics as a full-time Assistant Engineer. He is currently an Associate Professor at the Department of Mechanical Engineering, Hanyang University. His research interests include non-linear modeling of in-space manufacturing process, prognostics health, image segmentation with LiDAR, and quality monitoring/control in smart factory.

YOUNGKI KIM (Member, IEEE) received the B.S. and M.S. degrees in mechanical engineering from Seoul National University, South Korea, in 2001 and 2003, respectively, and the Ph.D. degree from the University of Michigan, Ann Arbor, MI, USA, in 2014.

From 2003 to 2008, he was a Research Engineer at Hyundai-Kia Motor Company. From 2015 to 2017, he was a Research Engineer at the Ann Arbor Technical Center, Southwest Research Institute, University of Michigan–Dearborn (UM–Dearborn), Dearborn, MI, USA. He is currently an Assistant Professor with the Department of Mechanical Engineering, UM–Dearborn. His research interests include modeling and estimation/control of electrified powertrain systems, connected and automated vehicles, and energy storage systems.

Dr. Kim was a recipient of the SAE Russell S. Springer Award by SAE International, in 2019.